Available online at www.sciencedirect.com
ScienceDirect
Polymer 47 (2006) 8053–8060
polymer
www.elsevier.com/locate/polymer

Transient crystallization during drawing from ultra-high molecular weight polyethylene melts having different entanglement characteristics

Masaki Kakiage [a], Takeshi Yamanobe [a], Tadashi Komoto [a], Syozo Murakami [b], Hiroki Uehara [a,*]

[a] *Department of Chemistry, Gunma University, Kiryu, Gunma 376-8515, Japan*
[b] *Department of Human Environment Design, Heian Jogakuin University, Takatsuki, Osaka 569-1092, Japan*

Received 22 March 2006; received in revised form 28 July 2006; accepted 30 July 2006
Available online 2 October 2006

Abstract

The relationship between entanglement characteristics and transient crystallization during drawing from ultra-high molecular weight polyethylene (UHMW-PE) melts is discussed, based on a combination of *in situ* X-ray measurement and stress profile analysis. Films having different entanglement characteristics were prepared by solution blending of higher and lower MW samples having a viscosity average MW of 1.07×10^7 (higher) and 1.73×10^6 (lower), followed by compression molding at 180 °C. Stress profiles recorded at 155 °C above the melting temperature of 135 °C exhibited a plateau stress region, whose stress level was lower for the film prepared with more of the lower MW component. With drawing, an amorphous scattering gradually concentrated on the equator. Beyond the beginning point of the plateau stress region, such amorphous scattering abruptly disappeared and crystallization into a transient hexagonal phase occurred simultaneously. As soon as this hexagonal phase appeared, it rapidly transformed into an orthorhombic phase for the film exhibiting higher plateau stress. In contrast, the film exhibiting lower plateau stress exhibited a gentle transformation and a resurgence of the hexagonal phase in the later stage of drawing. These results demonstrate that ''entanglement phase separation'' proceeds during melt-drawing of UHMW-PE.

Keywords: Ultra-high molecular weight polyethylene; Melt-drawing; Transient crystallization

1. Introduction

It has been reported that transient crystallization into the metastable form occurs within a short time scale of tens of seconds when some alkanes are crystallized from the molten state [1,2]. Polyethylene (PE) is a long alkane in which the same methylene units are propagated. However, PE usually crystallizes into the lamellar crystals without passing through the extended chain crystals, due to the restriction of chain mobility even in the melt. In contrast, it is known that the crystallization into the extended chain crystals of PE occurs under high temperature and pressure [3–8]. The crystal form of such extended chain crystals is the hexagonal phase, which is the most stable under these extended crystallization conditions. However, this hexagonal phase transforms into the normal orthorhombic phase as soon as cooling temperature or increasing pressure. Therefore, we consider that the phase transition from melt through hexagonal into orthorhombic modification is possible if the molecular orientation can be dynamically introduced into the molten state of PE.

We have demonstrated that transient crystallization similar to that of alkanes occurs even for PE when deformation is applied in the molten state [9]. Namely, tensile drawing from molten PE having an ultra-high molecular weight (UHMW) induces transient crystallization into a hexagonal phase, corresponding to a metastable form of alkanes, during oriented

* Corresponding author. Tel.: +81 277 30 1332; fax: +81 277 30 1333.
E-mail address: uehara@chem.gunma-u.ac.jp (H. Uehara).

0032-3861/$ - see front matter © 2006 Elsevier Ltd. All rights reserved.
doi:10.1016/j.polymer.2006.07.073

crystallization into a final orthorhombic phase. This transient crystallization into the hexagonal phase has been applied to the industrial processing of UHMW-PEs [10]. Nevertheless, a normal PE having a conventional MW of less than 10^6 g/mol cannot be melt-drawn [11]. Considering that the initial UHMW-PE melt contains numerous chain entanglements but that they are reduced during melt-drawing [12–14], it is predictable that such a transient crystallization mechanism is dominated by the changes in the entangled state of long molecules.

Therefore, in this study, we tried to compare the structural changes during drawing from a series of melts having different entanglement characteristics, i.e., average number of entanglements per chain. A comparison of these results will clarify the role of chain entanglements in transient crystallization for longer PE chains.

To prepare films having different entanglement numbers per chain, we used two UHMW-PEs polymerized by a metallocene catalyst with higher and lower MWs as the starting materials. These UHMW-PEs have a narrower MW distribution (MWD) than those obtained by the usual Ziegler catalyst system [15,16]. Thus, the blending of these metallocene-catalyzed UHMW-PEs yields a bimodal MWD with higher and lower MW peaks. Such materials, with less intermediate MW components, are expected to give results that predict the individual roles of higher and lower MWs in transient crystallization during melt-drawing.

The measurement setup is specially designed for the *in situ* analysis performed in this study. Usually, the structures of hot-drawn samples are analyzed under ambient conditions after they have been taken out of the drawing device. However, such a procedure will induce additional change through cooling crystallization, especially for melt-drawing, where the sample contains both the crystalline solid and an amorphous melt. Thus, *in situ* analysis is necessary for this study. We previously analyzed structural changes during solid-state drawing by using wide-angle X-ray diffraction (WAXD) [17]. Recently, a synchrotron radiation beam has been used for *in situ* WAXD analysis of structural change during processing including spinning [18–23], drawing [24–28] and flow [29–31]. The high luminescence of the synchrotron radiation beam enables us to detect the structural change with a very fine time scale. Such a high time-resolved analysis is especially powerful for detecting rapid phase changes like the transient crystallization targeted in this study.

Another *in situ* analysis we adopted for this study is a continuous stress measurement during melt-drawing. It is well known that the stress–strain behavior reflects the structural change during drawing. For this *in situ* stress measurement, our drawing device was specially configured by installing a load cell. A combination of these *in situ* analyses reveals the relationship between oriented crystallization and the deformation mechanism during melt-drawing. Similar simultaneous stress measurements with *in situ* WAXD analyses have been reported for drawing of UHMW-PE composite [32], rubber [33–38], polypropylene [39], poly(ethylene terephthalate) [40–42] and poly(3-hydroxy butyrate) [43].

2. Experiment

2.1. Initial materials

Two kinds of UHMW-PEs having different MWs but a narrower MWD were supplied by Asahi Kasei Chemicals Co. They were prepared using the metallocene catalyst system with viscosity average MWs (M_v) of 1.07×10^7 and 1.73×10^6. Gel permeation chromatography (GPC) measurements were carried out for these materials, but it is known that components having MWs over 10^7 are undetectable by the GPC method. Thus, accurate analysis of MWD was difficult, especially for the UHMW-PE having a higher M_v of 1.07×10^7.

2.2. Sample preparation

Four kinds of films were prepared with component ratios (wt%) of 100/0, 75/25, 50/50 and 0/100 for both the higher and lower M_v materials, as shown in Table 1. Appropriate amounts of these UHMW-PEs, 0.2 wt%, were dissolved in *p*-xylene at the boiling point under a nitrogen gas flow. Antioxidants, 0.5 wt% (based on polymer) of both octadecyl 3-(3,5-di-*tert*-butyl-4-hydroxyphenyl)propanoate and bis(2,4-di-*tert*-butylphenyl)pentaerythritol diphosphite, were added. A gel-like aggregation was precipitated by slow cooling to room temperature (RT), filtered into a mat, and then soaked in an excess amount of acetone for *p*-xylene exchange. The mats were dried at RT under a vacuum. The dried mats were compression molded into films at 180 °C and 30 MPa for 10 min, followed by slow cooling to RT. Before this molding procedure, a 0.5 wt% acetone solution of the above-mentioned antioxidants was applied to the surface of the dried mats. The resultant film thickness was ~0.7 mm. Their crystallinities were always around 50%, independent of the blend ratios, as shown in Table 1.

2.3. Melt-drawing

The drawing specimen was cut from these compression-molded films in a dumbbell shape, with the straight region 4 mm wide and 12.5 mm long. All melt-drawings were made at 155 °C, well above the sample melting temperature (T_m) shown in Table 1, by using a previously designed high-temperature extension device for *in situ* measurements [44,45]. A chamber covers the straight region of the dumbbell

Table 1
Component percentage and DSC characteristics of each blend film

Film	Component ratio (wt%)		Crystallinity (%)[a]	T_m (°C)[a]
	Higher M_v	Lower M_v		
100/0	100	0	49	134.6
75/25	75	25	50	134.4
50/50	50	50	52	134.2
0/100	0	100	57	134.5

[a] Evaluated by DSC measurement.

specimen. Before drawing, the sample specimen was held at 155 °C for 5 min for temperature equilibrating. The cross-head speed (CHS) of drawing was always 24 mm/min. The stress during such a melt-drawing process was recorded by using a load cell (Kyowa Electronic Instruments Co., Ltd., LUR-A-50NSA1) installed in the extension device.

2.4. Measurements

A Perkin Elmer Pyris 1 DSC was used for differential scanning calorimetry (DSC) measurements. Heating scans were preformed up to 180 °C at a rate of 10 °C/min under a nitrogen gas flow. The sample T_m was evaluated as the peak temperature of the melting endotherm. The temperature and heat of fusion (ΔH_f) were calibrated using indium and tin standards. Crystallinities were calculated from ΔH_f, assuming the ΔH_f of perfect PE crystals to be 290 J/g [46]. *In situ* WAXD measurements were carried out during the melt-drawing process by using a synchrotron radiation source at the BL40B2 beamline of SPring-8 (Japan Synchrotron Radiation Research Institute, Hyogo, Japan). Our extension device [44,45] was installed in the beamline, and WAXD images were continuously recorded during the melt-drawing process on a cooling-type CCD camera (Hamamatsu Photonics K.K., C4880). The wavelength of the synchrotron beam was 1.00 Å. The exposure time for each pattern was 1 s with a time interval of 5.5 s for date storage.

3. Results and discussion

We have previously reported that melt-drawing of UHMW-PE results in a unique stress–strain behavior [12–14], i.e., a plateau stress phenomenon, which is sensitive to the entanglement characteristics of the film. An easily disentangled melt exhibits lower stress and longer strain in the plateau region. In contrast, a tightly entangled one induces a higher plateau stress over a shorter strain range [12]. These results indicate that the entanglement characteristics are predictable from the differences in the plateau stress phenomenon. In the same way, the stress–strain behaviors of the films prepared in this study were evaluated at a constant drawing temperature of 155 °C, which well exceeds the end tail (~140 °C) of the DSC melting endotherms. Before drawing, the sample temperature was isothermally held at 155 °C for 5 min, resulting in a completely molten state, which could be confirmed by the homogeneously transparent appearance of the films. Here, the 100/0, 75/25 and 50/50 films could be melt-drawn at 155 °C, but the 0/100 film, composed only of the lower M_v component, was immediately broken as soon as the draw was initiated. Fig. 1 compares the stress profiles recorded during melt-drawing at 155 °C for the former three films prepared at different blend ratios. The horizontal axis for drawing time represents the sample strain because all draws were made at a constant CHS of 24 mm/min, corresponding to an average strain rate around 5 min^{-1} as estimated from the separation of pre-inked marks on the sample surface. The actual drawn region was the center region of the dumbbell sample with an initial length around 5 mm. All stress profiles exhibit a plateau stress region, but the stress level decreases as the blend ratio of the lower M_v component is increased. Meanwhile, the time period of the plateau stress region gradually elongates. Such changes in plateau stress phenomena are quite similar to those observed for easily or less easily disentangled melt in our previous study [12], as described above. This plateau stress means the melt viscosity, corresponding to the average number of entanglements per chain. A comparison of these results suggests that the melt viscosity gradually decreased as the blend ratio of the lower M_v component in the film is increased. Therefore, it is reasonably assumed that the average number of entanglements per chain is controllable by the blend ratio.

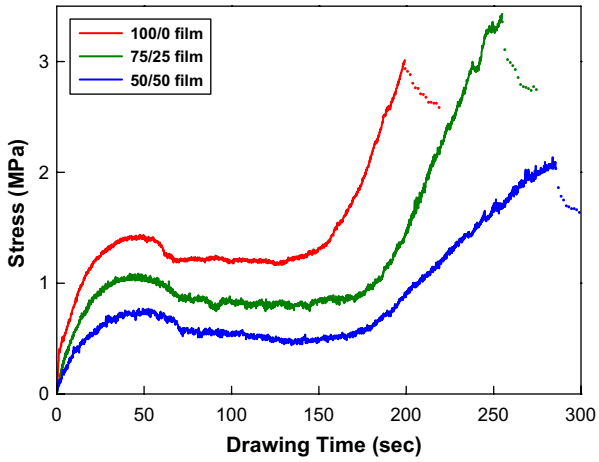

Fig. 1. Comparison of stress profiles recorded during melt-drawing at 155 °C for 100/0, 75/25 and 50/50 films.

After these plateau stress regions, the stress steeply increases with increasing strain. Such stress development in the later stage of melt-drawing corresponds to strain hardening [47]. Often, the strain-hardening phenomenon accompanies oriented crystallization, which has been reported for rubbers [34–37]. Here, it should be noted that these films deformed with no necking through all the strain regions, as confirmed by the changes in sample appearance recorded during melt-drawing. The elongation estimated from the separation of the pre-inked marks increased linearly with drawing time for all the films. These results suggest that homogeneous deformation proceeds during melt-drawing, independent of the sample films prepared in this study.

Structural changes during melt-drawing were characterized by *in situ* WAXD measurements using a synchrotron radiation source. In particular, the results obtained for the two films exhibiting the highest and lowest plateau stresses, i.e., the 100/0 and 50/50 films (see Fig. 1), were compared in order to evaluate the effects of entanglement characteristics on melt-drawing behavior. Fig. 2 depicts the stress profile of the 100/0 film at 155 °C and the corresponding change in the *in situ* WAXD patterns recorded during drawing. Before drawing, only non-oriented amorphous scattering is observed. Thus, the film is initially in a complete molten state. With drawing, the stress increases and amorphous scattering gradually concentrates on the equator. This means that amorphous chains

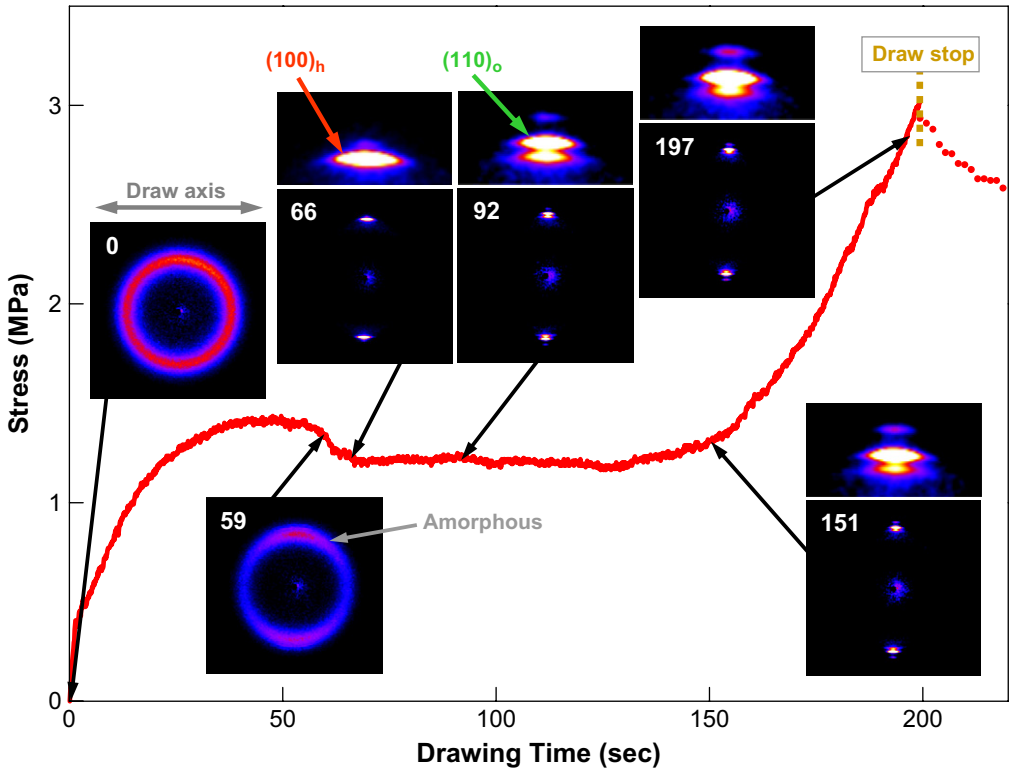

Fig. 2. Stress profile recorded at 155 °C with corresponding change of *in situ* WAXD patterns for 100/0 film. The draw direction for the WAXD patterns is horizontal. Subscripts "o" and "h" indicate the orthorhombic and hexagonal phases, respectively. Enlarged images of the crystalline reflection regions are shown on the upper side. The drawing time in seconds is indicated for each pattern.

orient in the direction of the drawing axis. However, no crystal reflection is detectable even at the yield point. When drawing proceeds up to the beginning of the plateau stress region beyond this yielding, the amorphous scattering abruptly disappears. Simultaneously, a strong hexagonal (100) reflection of arc shape appears on the equator. This hexagonal (100) reflection immediately begins to decrease just after its appearance. An orthorhombic (110) reflection then appears and gradually becomes stronger. These phenomena mean that the initial crystallization during melt-drawing proceeds in a "transient" hexagonal phase. After passing through the plateau stress region, the draw stress increases, but there are no significant changes in either of reflection intensity. Here, the converse transition from the orthorhombic into hexagonal form has been reported for heating process of the ultra-drawn high modulus PE [17,48–50]. For melt-drawing, the hexagonal phase appeared with the plateau stress, which could correspond to the constrained condition for the ultra-drawn high modulus PE. Regarding this phase transition from the hexagonal into the orthorhombic phase, the reversibility for this phase transition is interesting. In the future study, we are planning to examine the changes in the hexagonal phase for both relaxation and cooling processes after melt-drawing of PE.

A similar *in situ* analysis was carried out for melt-drawing of the 50/50 film exhibiting the lowest plateau stress value among the three films examined in this study (see Fig. 1). Fig. 3 illustrates the stress profile of the 50/50 film at 155 °C and the corresponding change in the *in situ* WAXD patterns recorded during drawing. The changes in the diffraction patterns before the yield point are similar to those for the 100/0 film (see Fig. 2). Namely, the amorphous chains orient before the yield point, but no crystal reflection is recognized. At the beginning point of the plateau stress region, the oriented amorphous scattering abruptly disappears and a hexagonal (100) reflection simultaneously appears on the equator. At this time, orthorhombic (110) reflection is not observed. These phenomena are quite similar to those of the 100/0 film. However, the difference lies in the later decrease of the hexagonal (100) reflection and the simultaneous increase of the orthorhombic (110) reflection. Both of these changes proceeded within the plateau stress region for the 50/50 film, but their significance is minor compared to those of the 100/0 film. With increasing draw stress beyond the plateau region, the arc-shaped orthorhombic (110) reflection gradually transforms into a spot-shaped one for the 50/50 film.

Quantitative analyses of these structural changes were made by comparing the line profiles extracted along the equators from the series of *in situ* WAXD patterns shown in Figs. 2 and 3. The obtained 2θ profiles are plotted as a function of drawing time in Figs. 4 and 5. The decrease in the sample thickness was less significant than the width reduction, thus the intensity correction for the geometrical change was not introduced. Changes in amorphous scattering in the early stage of the draw are similar for these profiles. Its intensity rapidly decreases when crystallization starts at the beginning point of the plateau stress region. However, further drawing results in

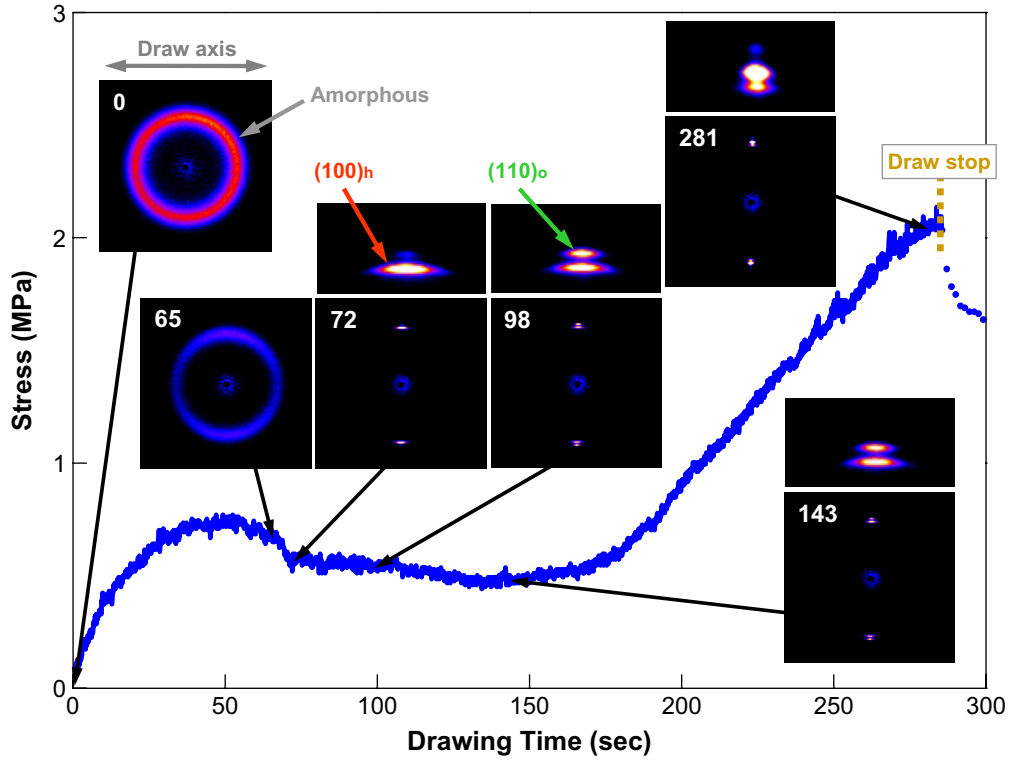

Fig. 3. Stress profile recorded at 155 °C with corresponding change of *in situ* WAXD patterns for 50/50 film.

a constant intensity of amorphous scattering. These phenomena are similar for both 100/0 and 50/50 films having different molecular entanglement characteristics.

In contrast, the changes in the crystalline reflections were quite different between the 100/0 and 50/50 films. As shown in Fig. 4, the strong hexagonal (100) reflection appears but immediately decreases just beyond the beginning point of the plateau stress region for the more entangled melt of the 100/0 film. A simultaneous increase in orthorhombic (110) reflection indicates that the crystal–crystal phase transition from the transient hexagonal phase into the resultant orthorhombic phase proceeds at a critical drawing time. For the less entangled 50/50 film shown in Fig. 5, the intensity of the initial hexagonal (100) reflection is obviously lower than that of the 100/0 film. Therefore, the transition into the later orthorhombic phase looks gentler. When the draw proceeds to the strain-hardening region, the hexagonal phase increases once again and transforms into the orthorhombic phase. Such a separate, duplicate transition from the hexagonal into the orthorhombic phase was not recognized during melt-drawing of the 100/0 film. These results indicate that the structural changes involving crystalline phases are strongly affected by the entanglement characteristics, i.e., the average number of entanglements per chain of the sample.

The differences in crystalline reflections between the 100/0 and 50/50 films were compared using their integral intensities to discuss the relationship between entanglement characteristics of the sample and phase development mechanisms during melt-drawing. The extracted 2θ profiles were resolved into amorphous scattering, hexagonal (100), and orthorhombic (110) and (200) reflection peaks using the Voigt function, which combines Lorentzian and Gaussian functions. Among these resolved peaks, the hexagonal (100) and orthorhombic (110) ones were chosen for the evaluation of each crystallization mechanism. Changes in the integral intensities of these two reflection peaks during melt-drawing are compared in Figs. 6 and 7. The plot of the former hexagonal (100)

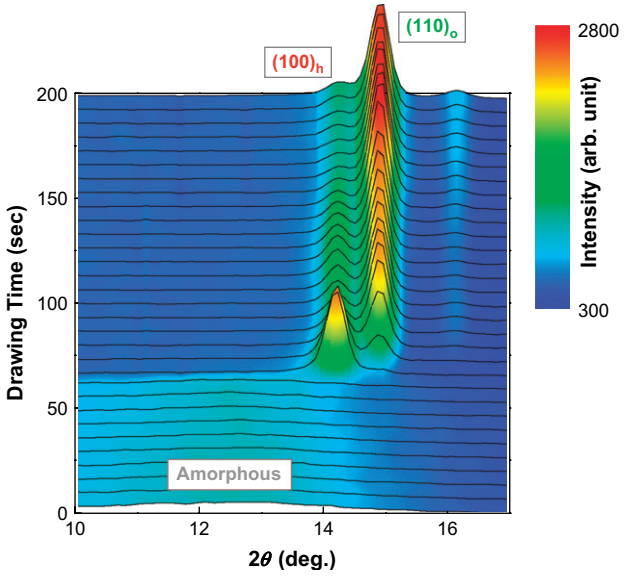

Fig. 4. 3D plot of WAXD line profiles extracted along the equators of the series of *in situ* WAXD patterns recorded during melt-drawing of 100/0 film at 155 °C.

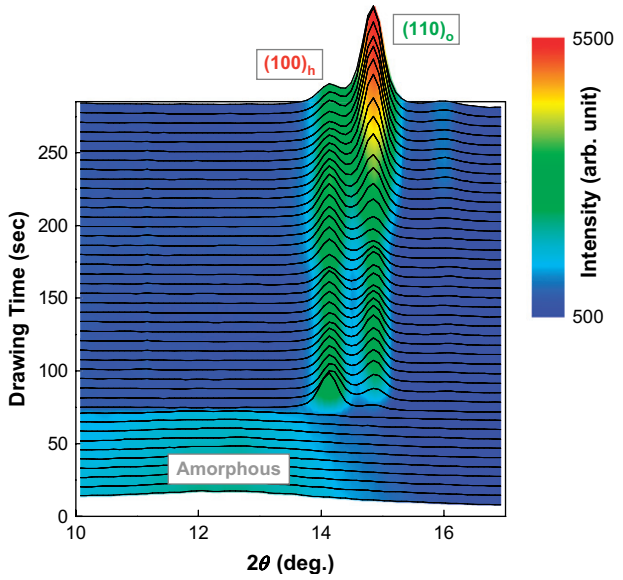

Fig. 5. 3D plot of WAXD line profiles extracted along the equators of the series of *in situ* WAXD patterns recorded during melt-drawing of 50/50 film at 155 °C.

reflection starts at the same drawing time, around 70 s, for both the 100/0 and 50/50 films, as shown in Fig. 6. This critical drawing time, at which crystallization into the hexagonal phase starts, is coincident with the beginning point of the plateau stress region in Fig. 1. When the initial values of the integral intensity of the hexagonal (100) reflection were compared for these two films, the higher value was obtained for the 100/0 film, which only contains a higher M_v component. Immediately after the hexagonal (100) reflection appears, its integral intensity drops. Meanwhile, that of the orthorhombic (110) reflection grows rapidly beyond this critical drawing time, as shown in Fig. 7. A combination of these phenomena suggests that the transition from the initial hexagonal phase into the resultant orthorhombic phase proceeds when the draw enters the plateau stress region. This means

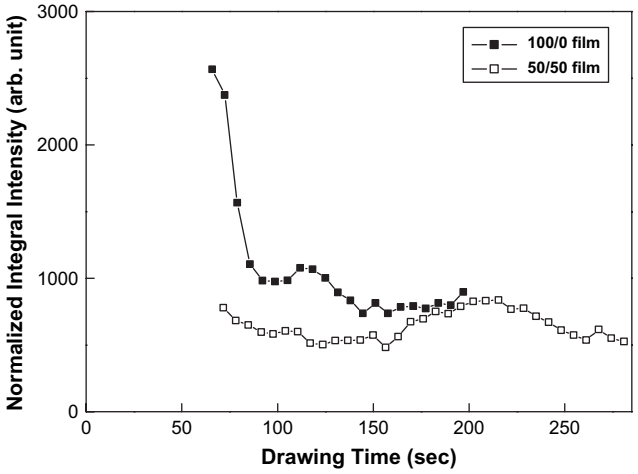

Fig. 6. Comparison of changes in integral intensities of the $(100)_h$ reflection peaks estimated from the series of WAXD line profiles shown in Figs. 4 and 5.

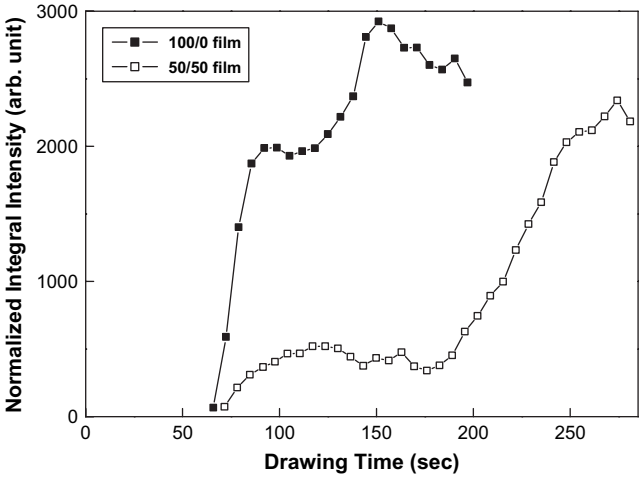

Fig. 7. Comparison of changes in integral intensities of the $(110)_o$ reflection peaks estimated from the series of WAXD line profiles shown in Figs. 4 and 5.

that transient crystallization into the hexagonal phase is induced at the initial stage of melt-drawing. In contrast, the 50/50 film exhibits a gradual decrease in the integral intensity of the hexagonal (100) reflection beyond this critical drawing time. Correspondingly, that of the orthorhombic (110) reflection also gradually increases during the early stage of the draw.

Another difference lies in changes during the later stage of draw, beyond 150 s. The 50/50 film exhibits a second increase in the integral intensity of the transient hexagonal (100) reflection. This drawing time corresponds to the entrance into the strain-hardening region (see Fig. 1). Further draw after this second critical drawing time reveals a decrease in the integral intensity of the hexagonal (100) reflection and a corresponding increase in the integral intensity of the orthorhombic (110) reflection. This phenomenon means that the transition from the former into the latter is the same as that observed at the first critical drawing time of around 70 s, i.e., transient crystallization during melt-drawing.

However, the increase in the integral intensity of the orthorhombic (110) reflection after the second critical drawing time is much more significant than that after the first critical drawing time for the 50/50 film. When the WAXD patterns obtained within the strain-hardening regions were compared between 100/0 and 50/50 films, broad arc-shaped reflections were observed for the former but concentrated spot-shaped ones were obtained for the latter. These results imply an ease of chain slippage for the less entangled component contained in the 50/50 film. The resultant high orientation of the orthorhombic chains produces a concentrated intensity on the equator, leading to a rapid increase in the integral intensities for the 50/50 film after the second critical drawing time.

Regarding the first and second increases in the integral intensity of the transient hexagonal (100) reflection occurring around 70 s and 150 s, the first increase is observable for both the 100/0 and the 50/50 films. Both of these films contain the higher M_v component. Thus, it can be expected that the component with the larger number of entanglements per chain induces abrupt crystallization in the early stage of draw. In

contrast, the second critical increase of the integral intensity of the hexagonal (100) reflection was recognizable only for the 50/50 film, which contains a lower M_v component. The narrower MWD of the metallocene-catalyzed UHMW-PEs used in this study enables us to distinguish these two routes for transient crystallization into the hexagonal phase. The balance of the two is dominated by the blend ratio of these UHMW-PEs, which controls the entanglement characteristics, i.e., the average number of entanglements per chain.

The effects of entanglement characteristics on phase changes during the melt-drawing process can be interpreted as follows. At the beginning point of the plateau stress region, the component with the larger number of entanglements per chain induces transient crystallization into the hexagonal phase. This hexagonal phase immediately transforms into an orthorhombic phase. At this moment, the less entangled component is in a molten amorphous state. Such component may be little contained for the 100/0 film. For the 50/50 film having the lower M_v component, the larger amount of this less entangled component induces a second crystallization into a transient hexagonal phase. In contrast, the 100/0 film does not exhibit this second transient crystallization phenomenon.

This logic predicts that ''entanglement phase separation'' occurs during melt-drawing for the 50/50 film. If the first transient crystallization is induced by the component with the larger number of entanglements per chain, the other entanglements are disentangled while passing through the plateau stress region. This means that separation of the two populations of entanglements having different characteristics has already proceeded before the critical drawing time, corresponding to the beginning of the plateau stress region. Such phase separation into melts with more and less entangled states takes place at the amorphous orientation region in the early stage of draw.

4. Conclusions

Transient crystallization during melt-drawing of UHMW-PE can be successfully detected by *in situ* WAXD measurements. With drawing, the orientation of the amorphous phase proceeded with no crystalline reflection. Subsequently, an abrupt crystallization into the hexagonal phase occurred at the beginning point of the plateau stress region, but it then transformed into the orthorhombic phase. The lifetime of this transient hexagonal phase is especially short, on the time scale of a few seconds, for more entangled melt prepared from the higher M_v component. In contrast, the hexagonal phase increased again at the later stage of draw for the film containing the lower M_v component, corresponding to a less entangled melt. These results indicate that the separation into more and less entangled components proceeds even before crystallization.

Acknowledgements

In situ WAXD measurement using synchrotron radiation was performed at the BL40B2 in the SPring-8 with the approval of the Japan Synchrotron Radiation Research Institute (JASRI) (Proposal No. 2003B0303-NL2b-np). We appreciate the cooperation of Drs. Masaru Kotera, Sono Sasaki and Katsuaki Inoue (JASRI). This work was partly supported by the Industrial Technology Research Grant Program in '04 from the New Energy and Industrial Technology Development Organization (NEDO) of Japan.

References

[1] Sirota EB, Herhold AB. Science 1999;283:529.
[2] Shinohara Y, Kawasaki N, Ueno S, Kobayashi I, Nakajima M, Amemiya Y. Phys Rev Lett 2005;94:097801.
[3] Wunderlich B, Arakawa T. J Polym Sci Part A 1964;2:3697.
[4] Bassett DC, Turner B. Nature Phys Sci 1972;240:146.
[5] Asahi T. J Polym Sci Polym Phys Ed 1984;22:175.
[6] Hikosaka M, Tsukijima K, Rastogi S, Keller A. Polymer 1992;33:2502.
[7] Rastogi S, Kurelec L, Lemstra PJ. Macromolecules 1998;31:5022.
[8] Kurelec L, Rastogi S, Meier RJ, Lemstra PJ. Macromolecules 2000;33:5593.
[9] Uehara H, Kakiage M, Yamanobe T, Komoto T, Murakami S. Macromol Rapid Commun 2006;27:966.
[10] Uehara H. Development of direct processing from polymer reactor powders using pelletize-less technique. NEDO technical report of Industrial Technology Research Grant Program, 00B68006d; 2002.
[11] Bashir Z, Keller A. Colloid Polym Sci 1989;267:116.
[12] Uehara H, Nakae M, Kanamoto T, Zachariades AE, Porter RS. Macromolecules 1999;32:2761.
[13] Nakae M, Uehara H, Kanamoto T, Ohama T, Porter RS. J Polym Sci Part B Polym Phys 1999;37:1921.
[14] Nakae M, Uehara H, Kanamoto T, Zachariades AE, Porter RS. Macromolecules 2000;33:2632.
[15] Razavi A. C R Acad Sci Paris Serie IIc 2000;3:615.
[16] Al-Hussein M, Davies GR, Ward IM. Polymer 2001;42:3679.
[17] Uehara H, Kanamoto T, Kawaguchi A, Murakami S. Macromolecules 1996;29:1540.
[18] Samon JM, Schultz JM, Wu J, Hsiao B, Yeh F, Kolb R. J Polym Sci Part B Polym Phys 1999;37:1277.
[19] Samon JM, Schultz JM, Hsiao BS, Seifert S, Stribeck N, Gurke I, et al. Macromolecules 1999;32:8121.
[20] Schultz JM, Hsiao BS, Samon JM. Polymer 2000;41:8887.
[21] Samon JM, Schultz JM, Hsiao BS, Wu J, Khot S. J Polym Sci Part B Polym Phys 2000;38:1872.
[22] Ran S, Burger C, Fang D, Zong X, Cruz S, Chu B, et al. Macromolecules 2002;35:433.
[23] Ran S, Burger C, Fang D, Zong X, Chu B, Hsiao BS, et al. Macromolecules 2002;35:9851.
[24] Samon JM, Schultz JM, Hsiao BS. Polymer 2000;41:2169.
[25] Ran S, Zong X, Fang D, Hsiao BS, Chu B, Phillips RA. Macromolecules 2001;34:2569.
[26] Wu J, Schultz JM, Samon JM, Pangelinan AB, Chuah HH. Polymer 2001;42:7141.
[27] Wu J, Schultz JM, Samon JM, Pangelinan AB, Chuah HH. Polymer 2001;42:7161.
[28] Yeh F, Hsiao BS, Sauer BB, Michel S, Siesler HW. Macromolecules 2003;36:1940.
[29] Goschel U, Swartjes FHM, Peters GWM, Meijer HEH. Polymer 2000;41:1541.
[30] Keum JK, Somani RH, Zuo F, Burger C, Sics I, Hsiao BS, et al. Macromolecules 2005;38:5128.
[31] Li L, de Jeu WH. Adv Polym Sci 2005;181:75.
[32] Chen X, Yoon K, Burger C, Sics I, Fang D, Hsiao BS, et al. Macromolecules 2005;38:3883.
[33] Murakami S, Senoo K, Toki S, Kohjiya S. Polymer 2002;43:2117.
[34] Toki S, Sics I, Ran S, Liu L, Hsiao BS, Murakami S, et al. Macromolecules 2002;35:6578.

[35] Toki S, Sics I, Ran S, Liu L, Hsiao BS. Polymer 2003;44:6003.
[36] Toki S, Sics I, Hsiao BS, Murakami S, Tosaka M, Poompradub S, et al. J Polym Sci Part B Polym Phys 2004;42:956.
[37] Tosaka M, Murakami S, Poompradub S, Kohjiya S, Ikeda Y, Toki S, et al. Macromolecules 2004;37:3299.
[38] Toki S, Sics I, Hsiao BS, Tosaka M, Poompradub S, Ikeda Y, et al. Macromolecules 2005;38:7064.
[39] Sakurai T, Nozue Y, Kasahara T, Mizunuma K, Yamaguchi N, Tashiro K, et al. Polymer 2005;46:8846.
[40] Kawakami D, Ran S, Burger C, Fu B, Sics I, Chu B, et al. Macromolecules 2003;36:9275.
[41] Kawakami D, Hsiao BS, Ran S, Burger C, Fu B, Sics I, et al. Polymer 2004;45:905.
[42] Kawakami D, Hsiao BS, Burger C, Ran S, Avila-Orta C, Sics I, et al. Macromolecules 2005;38:91.
[43] Iwata T, Fujita M, Aoyagi Y, Doi Y, Fujisawa T. Biomacromolecules 2005;6:1803.
[44] Murakami S, Tanno K, Tsuji M, Kohjiya S. Bull Inst Chem Res Kyoto Univ 1995;72:418.
[45] Murakami S. Nippon Kagaku Kaishi 2000;2:141.
[46] Wunderlich B, Cormier CM. J Polym Sci Part A-2 1967;5:987.
[47] Vincent PI. Polymer 1960;1:7.
[48] Pennings AJ, Zwijnenburg A. J Polym Sci Polym Phys Ed 1979;17:1011.
[49] Tashiro K, Sasaki S, Kobayashi M. Macromolecules 1996;29:7460.
[50] Ratner S, Weinberg A, Wachtel E, Moret MP, Marom G. Macromol Rapid Commun 2004;25:1150.